SUPPORTING INFORMATION

Multimodal Multiplexed Immunoimaging with Nanostars to Detect Multiple Immunomarkers and Monitor Response to Immunotherapies

Yu-Chuan Ou,[†] Xiaona Wen,[†] Christopher A. Johnson,[‡,§] Daniel Shae,[†] Oscar D. Ayala,[⊥] Joseph A. Webb,[†] Eugene C. Lin,[#,∥,¶] Rossane C. DeLapp,[□] Kelli L. Boyd,[■] Ann Richmond,[‡,§] Anita Mahadevan-Jansen,[⊥] Marjan Rafat,[†,⊥,△] John T. Wilson,[†,⊥,▲] Justin M. Balko,[▲,○] Mohammed N. Tantawy,[#,∥] Anna E. Vilgelm,[‡,§,●] and Rizia Bardhan[*,†,⊥,∥,⬡]

[†]Department of Chemical and Biomolecular Engineering, Vanderbilt University, Nashville, Tennessee 37235, United States

[‡]Department of Veterans Affairs, Tennessee Valley Healthcare System, Nashville, Tennessee 37212, United States

[§]Department of Pharmacology, Vanderbilt University School of Medicine, Nashville, Tennessee 37232, United States

[⊥]Department of Biomedical Engineering, Vanderbilt University, Nashville, Tennessee 37235, United States

[#]Radiology and Radiological Sciences, Vanderbilt University School of Medicine, Nashville, Tennessee 37232, United States

[∥] Vanderbilt University Institute of Imaging Science, Vanderbilt University School of Medicine, Nashville, Tennessee 37232, United States

[¶]Department of Chemistry and Biochemistry, National Chung Cheng University, Chiayi 62106, Taiwan

[□]Civil and Environmental Engineering, Vanderbilt University, Nashville, Tennessee 37235, United States

[■]Department of Pathology, Microbiology and Immunology, Vanderbilt University School of Medicine, Nashville, Tennessee 37232, United States

[△]Department of Radiation Oncology, Vanderbilt University School of Medicine, Nashville, Tennessee 37232, United States

[▲]Vanderbilt Center for Immunobiology, Vanderbilt University School of Medicine, Nashville, Tennessee 37232, United States

[○]Department of Medicine, Vanderbilt University School of Medicine, Nashville, Tennessee 37232, United States

[●]Department of Pathology, Ohio State University, Columbus, Ohio 43210, United States

[⬡]Department of Chemical and Biological Engineering, Iowa State University, Ames, Iowa 50012, United States

[*]Corresponding Author
E-mail: rbardhan@iastate.edu

Table of Contents

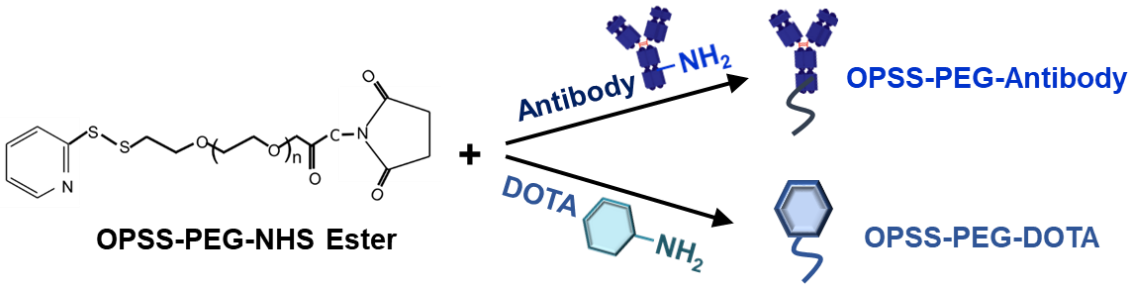

Scheme S1. Schematic describing modification of mAbs and DOTA for conjugation to IGNs. Antibodies and DOTA chelator were modified with a bifunctional linker OPSS-PEG2000-NHS ester forming an amide bond and terminating the PEG stabilized antibodies and chelator with a thiol *via* the orthopyridyl disulfide (OPSS) group. The free OPSS group is necessary to bind to gold surface of nanostars.

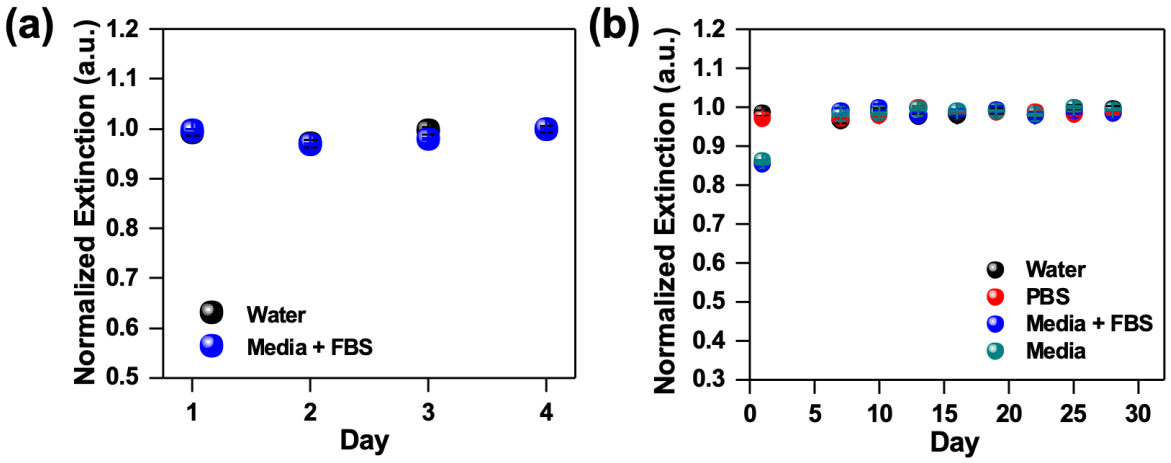

Figure S1. Stability and shelf life of IGNs. (a) Stability of IGNs in either water or media supplemented with fetal bovine serum (FBS) was studied by measuring the extinction spectra of IGNs. Normalized extinction showed minimal flocculation of IGNs. (b) Shelf life of IGNs was studied for four weeks. Aliquots of concentrated IGNs were dispersed in various media and the normalized extinction was measured over a month. IGNs were stored at 4 °C between measurements. Minimal change in extinction intensity indicates IGNs are highly stable and have excellent shelf life. The standard error in intensity of IGNs in various media was <0.008.

Table S1. IGN stability study. Full width at half maximum (FWHM) of extinction spectra of IGNs dispersed in either water or cDMEM. cDMEM = Dulbecco's modified eagle media supplemented with fetal bovine serum.

Day	H_2O (nm)	cDMEM (nm)
1	475	471
2	468	473
3	463	473
4	465	491

Table S2. Evaluation of IGN shelf life. Full width at half maximum (FWHM) of the extinction spectra of IGNs was tested in various media. Aliquots of IGNs were dispersed in various media and their stability was evaluated over four weeks. IGNs were stored at 4 °C in between measurements. PBS = phosphate buffered saline. cDMEM = Dulbecco's modified eagle media supplemented with fetal bovine serum. nDMEM = Dulbecco's modified eagle media without supplemented without fetal bovine serum.

Day	H_2O (nm)	PBS (nm)	cDMEM (nm)	nDMEM (nm)
1	492	504	487	465
7	486	481	479	476
10	484	482	483	467
13	467	517	474	467
16	495	505	480	474
19	519	521	480	474
22	522	520	488	472
25	521	516	478	474
28	521	527	481	475

A large increase (>10%) in the FWHM indicates aggregation of IGNs. IGNs are stable in all media with only small increase (~ 1 – 6% increase) in the FWHM over time.

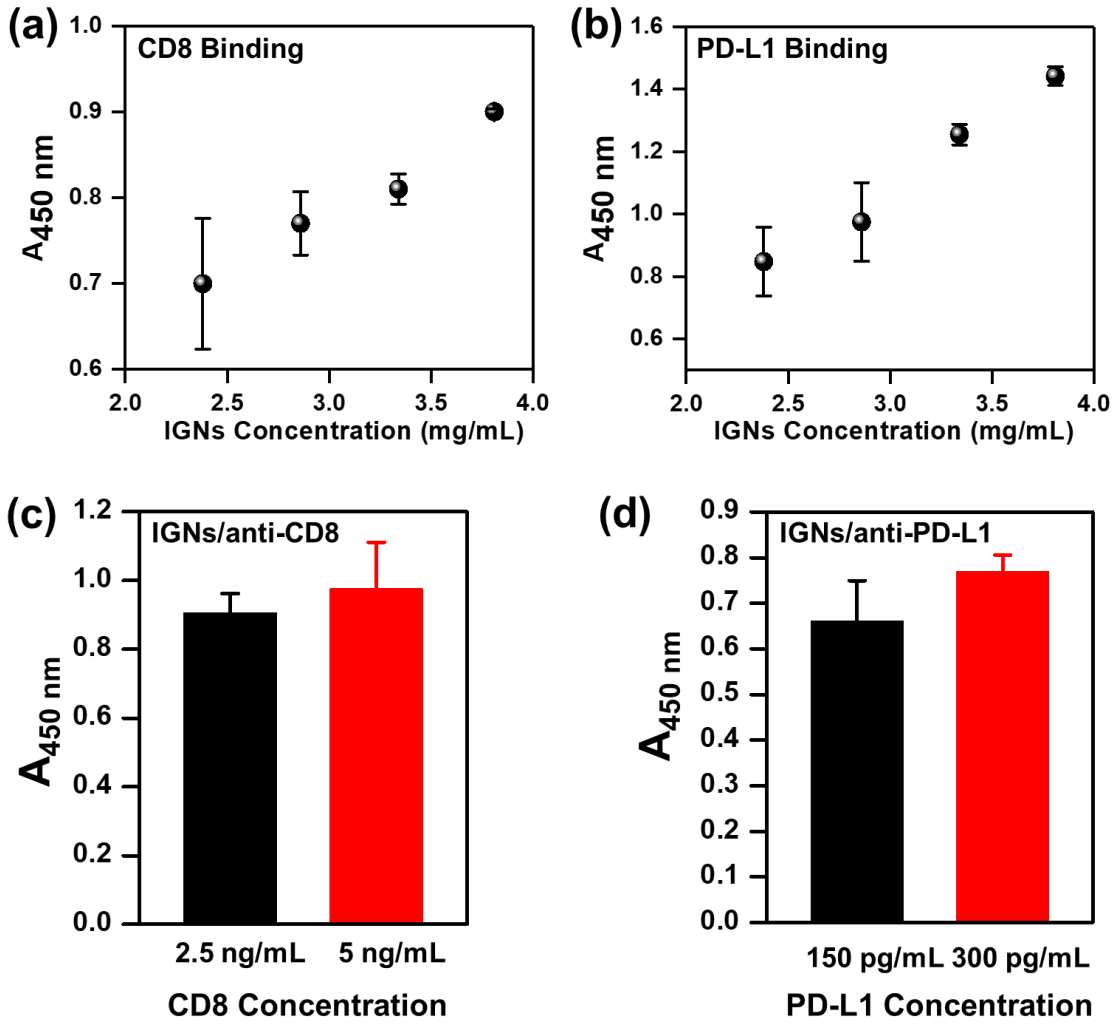

Figure S2. Binding study of antibody conjugated IGNs to respective antigen. (a) anti-CD8/IGNs binding assay to 5 ng/mL mouse CD8 antigen at increasing IGNs concentration. (b) anti-PD-L1/IGNs binding assay to 300 pg/mL mouse PD-L1 antigen at increasing IGNs concentration. (c) CD8 and (d) PD-L1 binding assay at two different concentrations with amount of IGNs held constant at 2.86 mg/mL.

In this binding assay, IGNs were used as a detection probe in the sandwich immunocomplex to show the successful binding of antibody conjugated IGNs to PD-L1 or CD8 antigen. We varied the amount of IGNs (Figure S2a,b) showing as more IGNs bound to the respective antigen, it resulted in higher signal from the secondary antibody (absorbance at 450 nm). The purpose of this experiment was to demonstrate that a higher PET and SERS signal *in vivo* is indicative of higher concentration of IGN binding as observed for mice in experimental group relative to control group in Figures 3 – 5. Next, we also held the IGNs concentration constant at 2.86 mg/mL and varied CD8 or PD-L1 antigen concentration. The purpose of this experiment was to demonstrate that mice (and ultimately translated to humans) with varied levels of PD-L1 and CD8 expression can be detected with our IGN probe. The results (Figure S2c,d) showed as expected trends where higher antigen concentration allowed more IGNs to bind giving rise to higher signal from the secondary antibody.

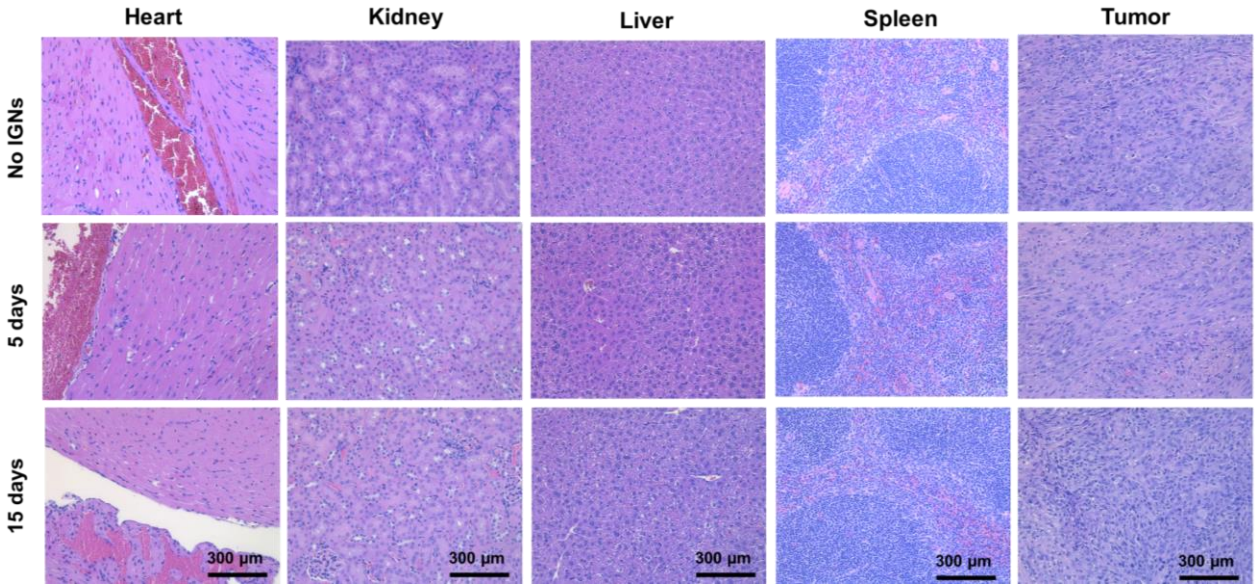

Figure S3. Hematoxylin and eosin (H&E) stain of heart, kidney, liver, spleen, and tumor to evaluate toxicity of IGNs. H&E stain of mice tissues showed IGNs did not cause any toxicity. Here, "No IGNs" control group represents mice tissues that received no treatment or IGNs dose.

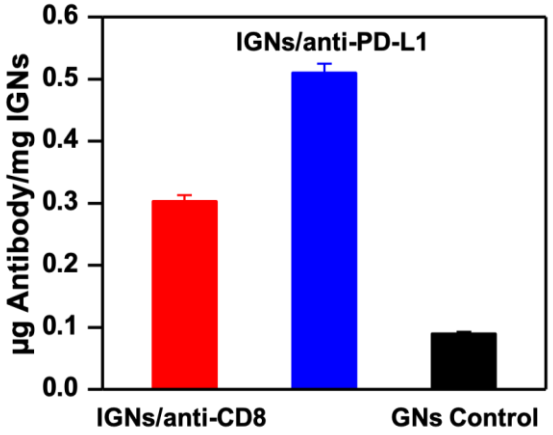

Figure S4. ELISA performed to quantify the number of monoclonal antibodies conjugated on nanostars surface when designing IGNs/DTNB/anti-CD8 and IGNs/pMBA/anti-PD-L1 relative to PEG conjugated nanostars control.

Table S3. Quantitative ICP-MS analysis of biodistribution of IGNs in YUMM 2.1 tumor-bearing mice 5 and 15 day post IGN delivery. Errors were measured from n = 3 mice for each time point.

Organ	*Time after IGN Injection (d)*	
	5 (μg Au/g tissue)	15 (μg Au/g tissue)
Muscle	2.1 ± 0.8	3.1 ± 2.6
Tumor	35.6 ± 21.0	24.3 ± 12.9
Brain	0.5 ± 0.2	0.9 ± 0.5
Lung	8.1 ± 1.2	16.5 ± 4.0
Stomach	18.3 ± 4.6	31.7 ± 8.8
Heart	21.2 ± 5.2	33.6 ± 2.6
Kidney	51.2 ± 11.5	62.4 ± 4.8
Spleen	505.0 ± 59.0	366.4 ± 138.2
Liver	187.9 ± 46.2	125.9 ± 71.0

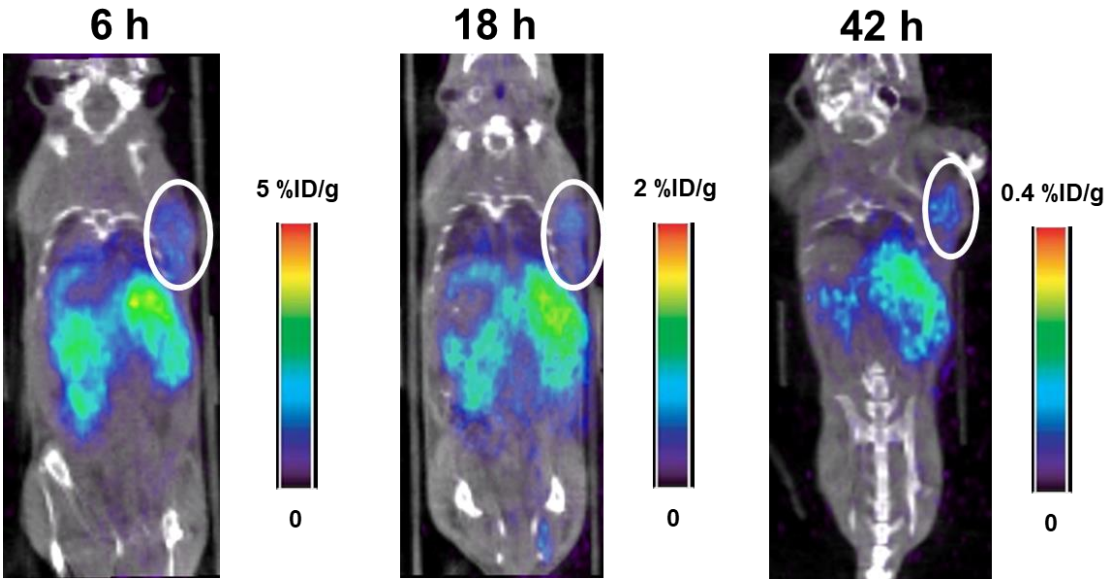

Figure S5. Whole body PET/CT images of blocked control mouse bearing YUMM 2.1 tumors. Receptors were blocked with mAbs prior to delivery of IGNs. Tumors are indicated with a circle.

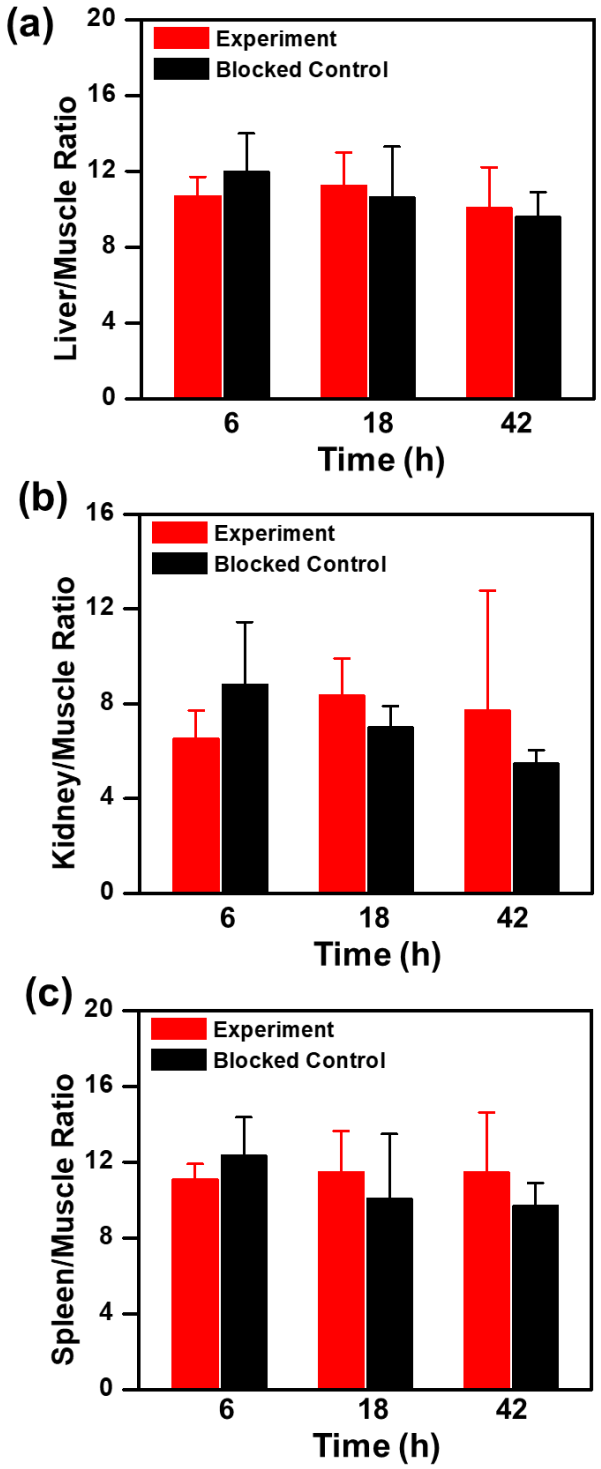

Figure S6. Quantification of PET signal in major organs, (a) liver to muscle ratio, (b) kidney to muscle ratio, and (c) spleen to muscle ratio (n = 4 for both experimental and blocked control groups). Statistical analysis was performed with student t-test and the differences here for liver, kidney, and spleen were statistically not significant (n.s.) for a – c.

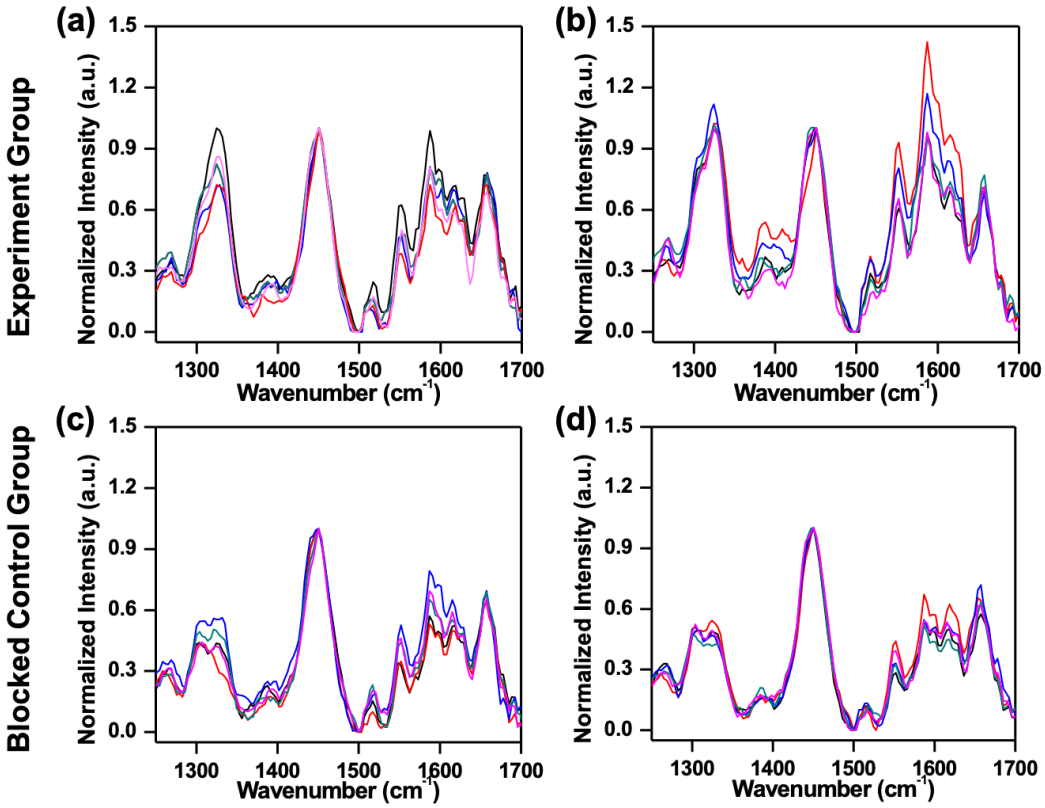

Figure S7. Examples of individual spectrum acquired from different locations of tumor for each mouse. (a,b) Two different mice from the experimental group shown in Figure 3 in main text. (c,d) Two different mice from the blocked control group.

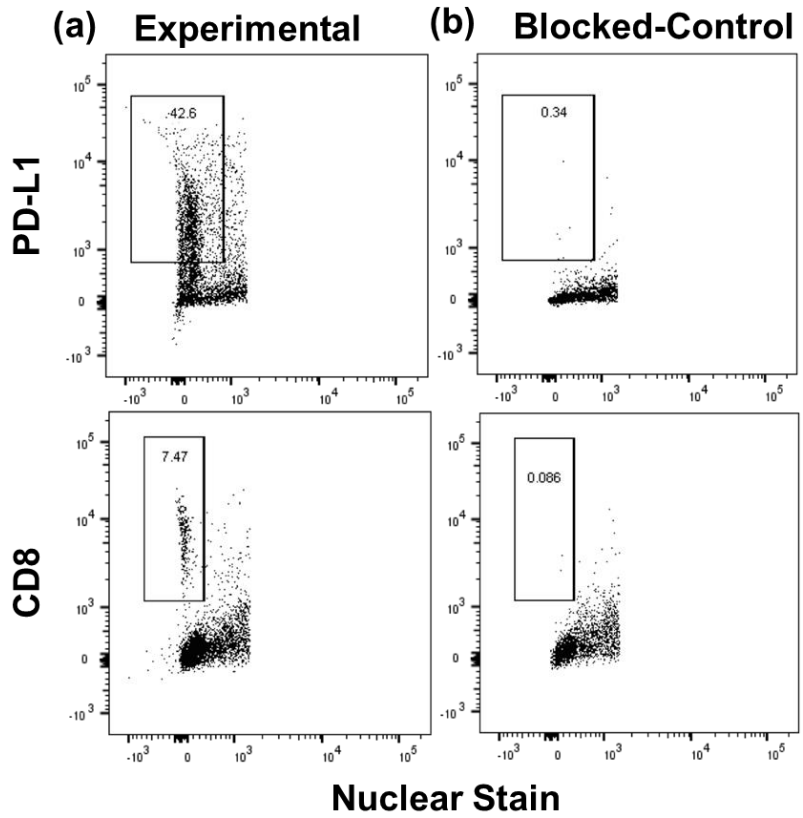

Figure S8. Flow cytometry of YUMM 2.1 tumors. Experimental tumors are both PD-L1 and CD8 positive (n= 3). Mice in the blocked control group that received anti-PD-L1 and anti-CD8 blocking antibodies showed significantly less PD-L1 and CD8 positive cells (n = 3).

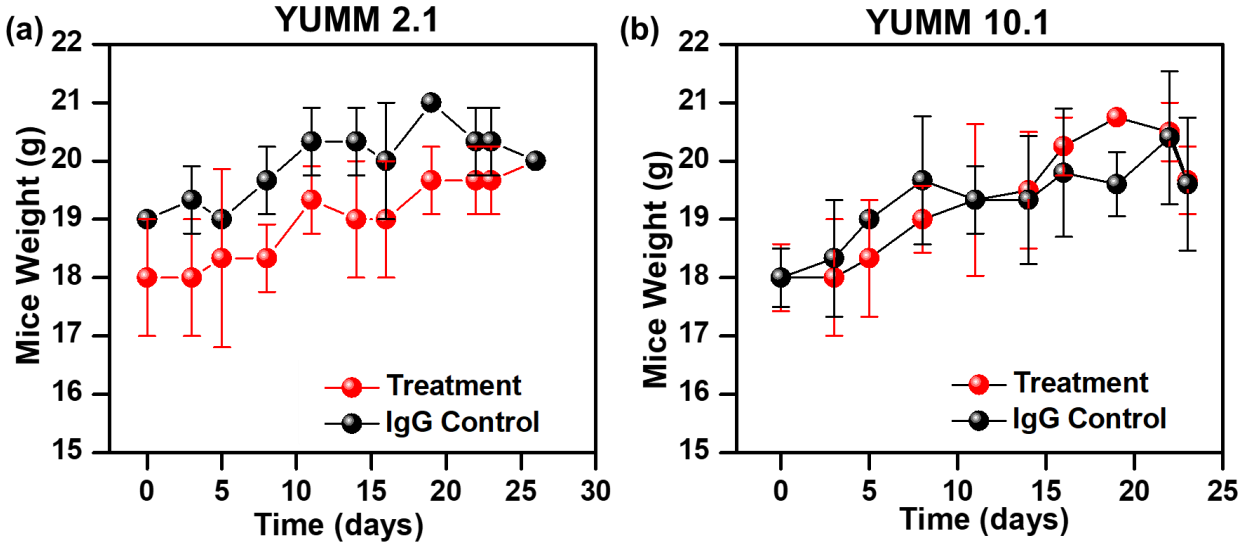

Figure S9. Mouse weight for both the control group and treated group (anti-CD137 + anti-PD-L1 combination therapy) for mouse bearing (a) YUMM 2.1 (n = 7 for treatment and control groups) and (b) YUMM 10.1 (n = 9 for both groups) tumor model.

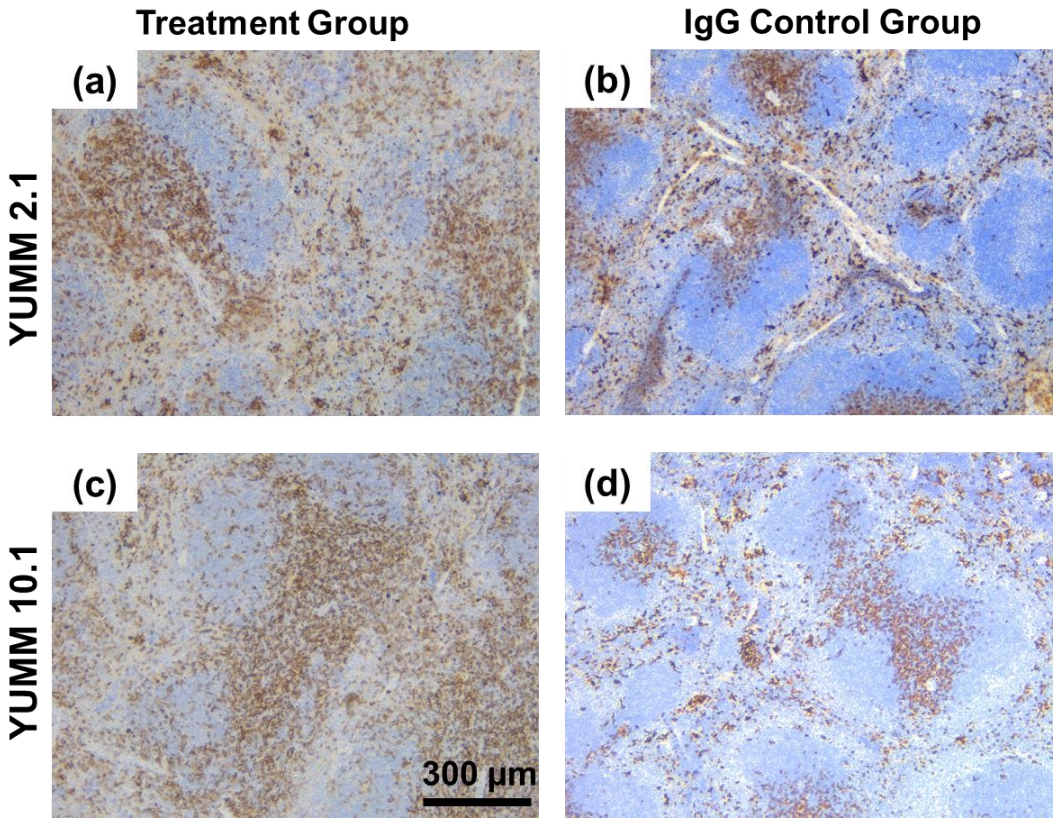

Figure S10. Immunohistochemistry staining for $CD8^+$ cells in the spleen of (a,c) treatment group (anti-CD137 + anti-PD-L1 combination therapy) and (b,d) control group mice. Scale bar is consistent (a) through (d).

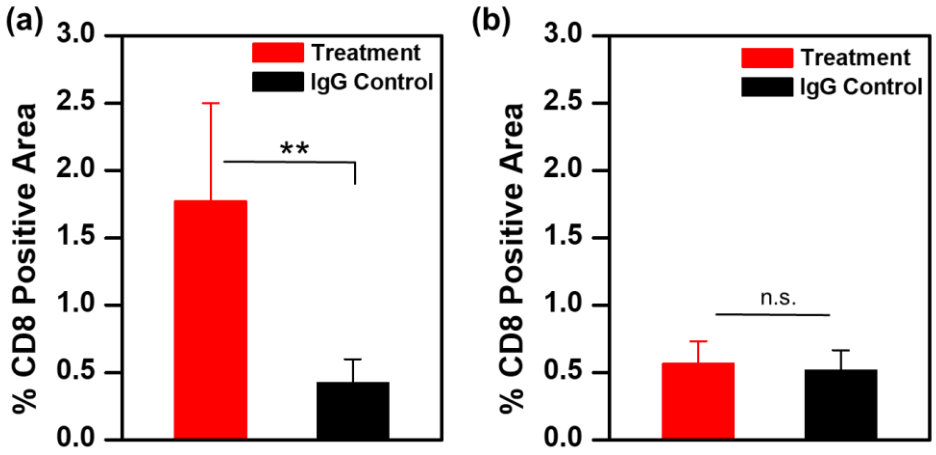

Figure S11. Quantification of $CD8^+$ intensity of tumors processed through immunohistochemistry of (a) YUMM 2.1 tumors (n = 5 treatment group, n = 4 control group,) and (b) YUMM 10.1 tumors (n = 4 control group, n = 5 treatment group). Here, ** indicates $p \leq 0.01$, and n.s. indicates not significant obtained with student t-test statistical analysis.

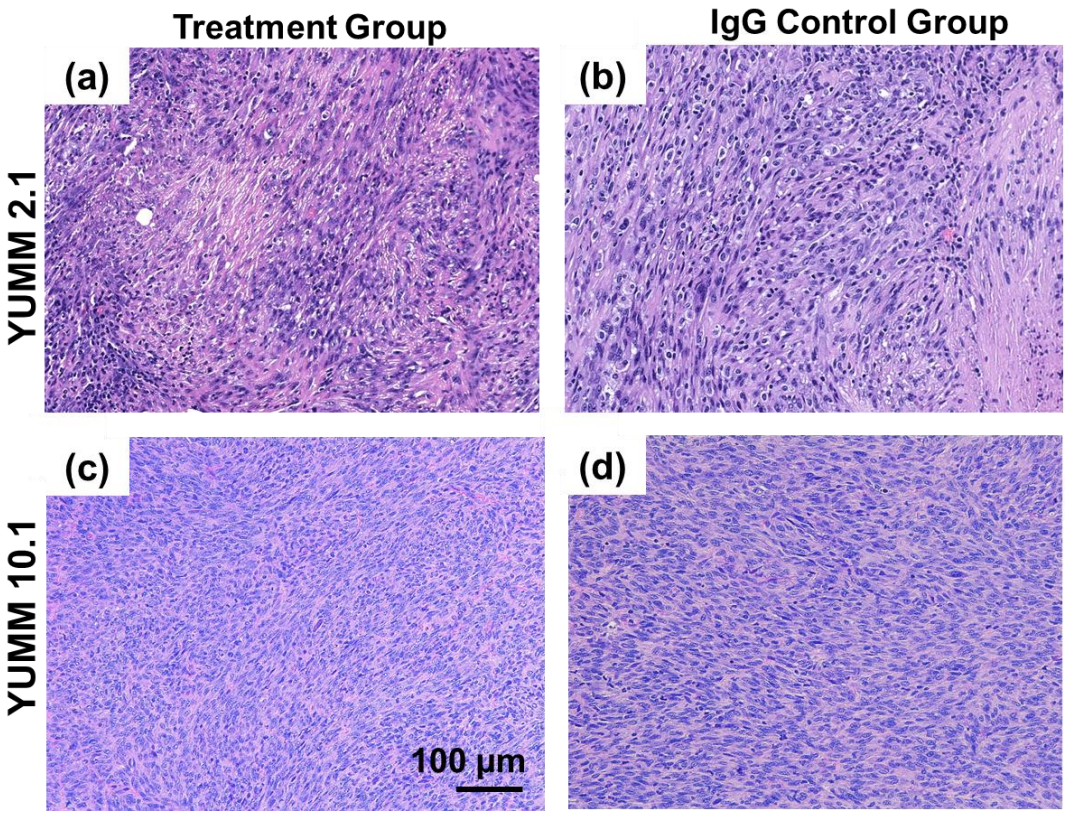

Figure S12. Hematoxylin and eosin (H&E) staining of tumor sections for the (a,c) treatment group (anti-CD137 + anti-PD-L1 combination therapy), and (b,d) IgG control group for YUMM 2.1 and 10.1 tumors. Scale bar is consistent (a) through (d).